14

Electronic Transport in Graphitic Carbon Nanoribbons

Eduardo Costa Girão,[a] Liangbo Liang,[b] Jonathan Owens,[b] Eduardo Cruz-Silva,[b,c] Bobby G. Sumpter,[d] and Vincent Meunier[b]
[a]*Departamento de Física, Universidade Federal do Piauí, Brazil*
[b]*Department of Physics, Applied Physics, and Astronomy, Rensselaer Polytechnic Institute, USA*
[c]*Department of Polymer Science and Engineering, University of Massachusetts, USA*
[d]*Center of Nanophase Materials Sciences, Oak Ridge National Laboratory, USA*

UNCORRECTED PROOFS

14.1 Introduction

Known carbon nanostructures span all four spatial dimensionalities and exhibit properties intimately related to different expressions of quantum spatial confinement. The discovery of fullerenes (0D) [1], carbon nanotubes (1D) [2], and the more recent experimental isolation of graphene sheets (2D) [3] have complemented the allotrope family tree long occupied by the centuries-old 3D forms of carbon (graphite and diamond). Discoveries made over the past 30 years have unveiled a number of emerging phenomena and paved the way to the possibility of devising a spectrum of diverse carbon nanostructures where elementary low-dimensional building blocks are assembled into systems with ever-increasing complexity. For instance, the most recent isolation of graphene from graphite has triggered an unprecedented material science research activity in the study of a wide variety of graphene derivatives, such as graphitic nanoribbons (GNRs).

At the same time as new materials are discovered and characterized, the confluence of scalable mathematical algorithms, novel electronic structure methods, advanced computing tools and exascale computational performance has enabled the development of predictive

Graphene Chemistry: Theoretical Perspectives, First Edition. Edited by De-en Jiang and Zhongfang Chen.
© 2014 John Wiley & Sons, Ltd. Published 2014 by John Wiley & Sons, Ltd.

tools for the discovery of novel phenomena, and principles for the design of new molecular electronics with breakthrough properties. In that respect, theoretical methods have now evolved to a point where the properties of materials can be successfully predicted based essentially on their atomic structure and with limited or no experimental input. As a consequence, computational science capabilities can substantially accelerate the search for novel materials and devices, especially when integrated with experimental effort. Enabled by these computational capabilities, exploration of how atomic scale structure and quantum mechanical effects impact electron transport and other electronic processes within nanostructures and across interfaces, provides critical information for developing the next generation of materials and electronic devices. In this chapter we review recent progress in describing electron transport in graphitic nanoribbons (GNRs) from a theoretical and computational perspective and how works published in the literature provide unique physicochemical insight that is applicable to the development of novel materials and devices.

The rest of this chapter is organized as follows: we review general theoretical framework for electronic structure and transport calculations in Section 14.2, we introduce the general properties of GNRs in Section 14.3, provide a short overview of synthesis and processing approaches in Section 14.4, then show how transport properties can be tailored for targeted applications in Section 14.5. We conclude this chapter with an overview of the current understanding of thermoelectric properties in GNRs in Section 14.6.

14.2 Theoretical Background

14.2.1 Electronic Structure

14.2.1.1 Density Functional Theory

Density functional theory (DFT) treats systems, in principle, on the basis of the ground state electron density. While this approach reduces the N-body problem from the determination of a many-body wave-function depending on 3N variables to a simpler three-variable density, approximations must be made in the expression of exchange and correlation, for which a number of local, semi-local, and non-local expressions exist. This allows the practical treatment of systems made up of hundreds of carbon atoms. As such, DFT has been widely used to study carbon nanostructures, including GNRs where spin-polarized DFT is typically needed to investigate edge effects. Unfortunately DFT is a ground state theory which cannot strictly be used to compute electronic band gaps without using post-DFT treatments such as quasi-particle GW. Reviews on density functional theory (DFT) can be found in a number of places, including the recent review by two of the present authors [4]. Thus, we will redirect the interested readers to the literature on DFT and elaborate on semi-empirical methods that make it possible to study larger systems (typically thousands of atoms) in a more systematic way. However, DFT remains the method of choice to establish new phenomena and to benchmark results obtained using those semi-empirical approaches.

14.2.1.2 Semi-Empirical Methods

Tight-binding (TB) calculations are known to provide a good description of the electronic properties of carbon based materials [5, 6], especially for geometries with moderate to

UNCORRECTED PROOFS

low curvature. TB can be made very accurate (e.g., compared to DFT) when considering high-order neighbor interactions [7,8] and enables simulation of very large systems [9]. For sp^2 carbon systems, it is usual to restrict the basis set to an orthogonal basis involving only the π-orbitals. This works particularly well in flat systems where the remaining orbitals are involved quasi-exclusively in forming the strong σ-bonds and are essentially decoupled from the π-orbitals. It follows that the major features of the electronic states close to the Fermi level have a strong π-character [10]. This π-orbital description implicitly considers that carbon atoms on the edges are saturated with hydrogens. The tight-binding hopping integrals are usually fit to experimental data or *ab initio* calculations [7,8]. For instance, the third-neighbor parametrization proposed by Gunlycke and White with $\gamma_1 = 3.2$ eV, $\gamma_2 = 0$ eV and $\gamma_3 = 0.3$ eV for the first-, second-, and third-nearest neighbor hopping integrals, respectively, was recently shown to result in an excellent agreement with DFT calculations for a varied set of systems [8, 11]. Finally, the different carbon coordination number at the edges is satisfactorily accounted for by including a $\Delta\gamma_1 = 0.2$ eV correction to the γ_1 parameter for the frontier atoms [8]. The various hopping integrals are schematically defined in Figure 14.1.

While spin-orbit and hyperfine couplings are weak in light elements such as carbon [12–14], it is also known that non-spin-polarized zigzag edges in graphene present an unstable high charge density which can be resolved by electronic charge polarization [15]. The proper description of the physics of edge states is fundamental to the successful development of nanodevices based on carbon nanoribbons as they can play a dominant role not only in infinite crystalline systems [15–17], but also in small finite-sized structures [18–20]. Such border effects persist in long one-dimensional systems even for lengths longer than 70 nm [18]. It follows that a correct description of zigzag edges in graphene must include spin interactions.

The addition of a Hubbard-like term to the Hamiltonian has been successful in describing the most relevant physical aspects of magnetic states in a number of graphitic carbon nanostructures, including finite nanoislands [21], where the results are shown to be consistent with Lieb's theorem [22]. Fundamental aspects of defect-induced magnetism in graphene and GNRs [23] as well as the magnetic states of zigzag edged GNRs [14, 15, 24] are also

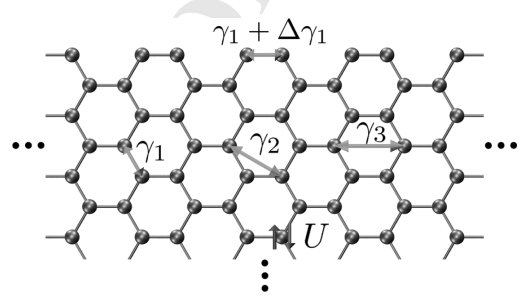

Figure 14.1 *Schematic representation of the first-, second-, and third-nearest neighbor hopping integrals (γ_1, γ_2 and γ_3, respectively) on an armchair edged graphitic structure. The different chemical environment at the edges is accounted for by a modified first neighbor interaction for these frontier atoms*

captured by such a simple approach. The Hubbard Hamiltonian $\hat{H}_U$ is written in terms of the number operators $\hat{n}_i^{\uparrow}$ and $\hat{n}_i^{\downarrow}$ for the spin-orbitals from atom i as:

$$\hat{H}_U = U \sum_i \hat{n}_i^{\uparrow} \hat{n}_i^{\downarrow}, \tag{14.1}$$

where the single parameter U corresponds to the on-site repulsion. Due to the complexity of solving this equation, a mean-field interaction is usually employed and this Hamiltonian is written as:

$$\hat{H}_U = U \sum_i \left(\langle \hat{n}_i^{\uparrow} \rangle \hat{n}_i^{\downarrow} + \hat{n}_i^{\uparrow} \langle \hat{n}_i^{\downarrow} \rangle \right) \tag{14.2}$$

where the densities $\langle \hat{n}_i^{\uparrow} \rangle$ and $\langle \hat{n}_i^{\downarrow} \rangle$ are determined self-consistently. A value of $U = 0.92\gamma_1$ as determined from DFT calculations reported Ref. [11]. The resulting tight-binding+U (TBU) model is then used to predict properties of GNRs. Results show a remarkable and systematic agreement between DFT and TBU for states close to the Fermi energy.

14.2.2 Electronic Transport at the Nanoscale

When describing electronic transport at the nanoscale, we take advantage of the fact that the device size is typically smaller than the phase coherence length [25, 26]) and quantum interference effects become prominent, demanding a full departure from the macroscopic description of Ohm's law. In a perfect crystalline system like a pristine GNR, for instance, electrons transmit through the system without suffering collisions, thereby marking a clear manifestation of ballistic transport. When we relax the defect free assumption (by considering doping and other structural defects like vacancies or reconstructions), electrons traveling through the system experience scattering events, thereby increasing the probability that some electrons will not be transmitted. Hence, a complete description of the transport at the nanoscale has to consider the transmission and reflection of the electronic waves. These aspects are captured by the Landauer formalism, which results in the following equation for the conductance G between two terminals (labeled by n and m) in the low bias and zero temperature limits [27, 28]:

$$G^{n \to m} = \frac{2e^2}{h} \mathcal{T}^{n \to m}. \tag{14.3}$$

where $\mathcal{T}$ is the transmission function. This result expresses the main tenet of the formalism, namely that *conductance is transmission*. This theory contains the essence of electronic transport at the nanoscale and marks a clear departure from the classical top-down description of electronic transport. As a result, Landauer's theory is today a widely used formalism for computing electronic transport properties of nanoscale systems with the aid of Green's function theory.

When performing a transport calculation, we consider a basic system made up of a central scattering region ($\mathcal{C}$) in contact with a number N of semi-infinite terminals ($\mathcal{L}_l$, $l = 1, 2, \ldots, N$) as depicted in Figure 14.2. Each terminal is composed by the repetition of a characteristic unit along a specific (periodic) direction.

The terminals do not need to be identical and we assume that each of the terminal's layers is indistinguishable from one in the corresponding bulk system. In addition, it is usual to

UNCORRECTED PROOFS

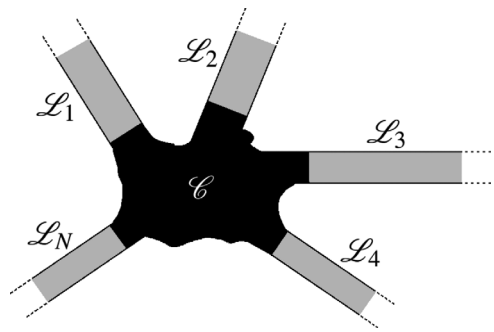

Figure 14.2 *Basic system for electronic transport calculations. A central scattering region $\mathcal{C}$ coupled to the semi-infinite terminals $\mathcal{L}_1$, $\mathcal{L}_2$, $\mathcal{L}_3$, $\mathcal{L}_4, \ldots, \mathcal{L}_N$*

adopt the principal layer (PL) concept to the electrodes, so that the terminal's PL is defined in such a way as to interact only with the first-neighboring cells. This allows the problem to be written in a convenient and numerically tractable way. In practice, Green's functions (GFs) provide a systematic way to determine the quantum transmission for the Landauer formula. Even though the Hamiltonian for the extended open system is infinite and non-periodic, we can still treat the conductor's GF (G_C) in terms of a modified Hamiltonian representing the central conductor by:

$$G_C^{r,a} = \Big((E \pm i\eta)I_C - H_C - \sum_l \Sigma_l\Big)^{-1} \tag{14.4}$$

with:

$$\Sigma_l = h_{Cl} g_l h_{lC}, \quad g_l = (\epsilon I_l - H_l)^{-1}, \tag{14.5}$$

where $\eta \to 0^+$ is a small complex number added to (subtracted from) the energy to avoid singularities in the calculation of the retarded (advanced) GF. Here, H_C (H_l) [h_{Cl} and h_{lC}] is the Hamiltonian describing $\mathcal{C}$ ($\mathcal{L}_l$) [the interaction between $\mathcal{C}$ $\mathcal{L}_l$] and the so-called self-energy matrices (Σ_i) can be interpreted as effective potentials which describe the effects of the semi-infinite terminals on $\mathcal{C}$. In other words, the sum of the H_C Hamiltonian with the self-energies represents a finite central conductor satisfying the boundary conditions corresponding to the extended system [27, 28]. The Hamiltonian matrices are obtained by *tight-binding*, that is, from a properly truncated DFT or TB calculation performed in a localized basis. Even though the Σ_l terms depend on infinite matrices when they are expressed in a localized-basis, we can write them in terms of finite matrices describing the interface between $\mathcal{C}$ and the first PL of $\mathcal{L}_l$ and determine them by recursive methods [29, 30]. Finally, the quantum transmission is obtained by [27, 28]:

$$\mathcal{T}^{n\to m} = Tr\big(\Gamma_n G_C^r \Gamma_m G_C^a\big), \tag{14.6}$$

with:

$$\Gamma_l = i(\Sigma_l - \Sigma_l^\dagger). \tag{14.7}$$

UNCORRECTED PROOFS

Conductance curves such as those reproduced in this chapter are computed using the equations provided in this section. Furthermore, using GF theory, we can attain insight into the profile of the charge flow by plotting the local current. The current I_{ij} between any two atomic sites, i and j, can be calculated with the aid of the GF ($G^<$) with [31, 32]:

$$I_{ij} = \frac{e}{h}\int_{-\infty}^{\infty} dE\Big(t_{ij}G^<_{ji}(E) - t_{ji}G^<_{ij}(E)\Big), \tag{14.8}$$

where $t_{ij} = t^*_{ji}$ is the hopping between sites i and j. In the absence of electronic correlations, $G^<$ is directly obtained from the retarded GF (G^r) by:

$$G^<(E) = G^r\Sigma^< G^{r,\dagger}; \qquad \Sigma^< = \sum_l f_l(\Sigma_l^\dagger - \Sigma_l), \tag{14.9}$$

where the sum runs over all the terminals, and f_l is the corresponding Fermi distribution used to fill the terminal states according to the chemical potential μ_l.

To ease the visualization of the local current data, we represent the local current in a real space representation:

$$I(x, y) = \sum_{i\neq j} \alpha_{ij}\langle \mathbf{r}|i\rangle\langle i|I|j\rangle\langle j|\mathbf{r}\rangle, \tag{14.10}$$

where $\langle i|I|j\rangle = I_{ij}$ and $\langle \mathbf{r}|i\rangle = e^{-r^2/a_{CC}^2}$ with r being the distance from the point (x, y) to the position of site i. As $I_{ij} = -I_{ji}$ (see Eq. 14.8), we select only the positive values of I_{ij} by setting $\alpha_{ij} = 1$ (0) when $I_{ij} \geq 0$ ($I_{ij} < 0$).

14.3 From Graphene to Ribbons

14.3.1 Graphene

Graphite is an abundant and well-known material. Yet, its isolation into individual *graphene* sheets was only accomplished in 2004 [3]. This result marked the starting point of intense research on both experimental and theoretical investigations, making graphene a focal point in materials science. Graphene's structure is composed of a honeycomb lattice, where carbon atoms are arranged on a bidimensional hexagonal motif. Its electronic structure can be accurately described within a tight-binding model. Setting $E_F = 0$ we write:

$$E(\mathbf{k}) = \pm\gamma\sqrt{3 + 2\cos\mathbf{k}\cdot\mathbf{a}_1 + 2\cos\mathbf{k}\cdot\mathbf{a}_2 + 2\cos\mathbf{k}\cdot(\mathbf{a}_1 - \mathbf{a}_2)}. \tag{14.11}$$

where $\mathbf{a}_1$ and $\mathbf{a}_2$ are graphene lattice vectors and $\mathbf{k}$ is a quasi-momentum chosen in the first Brillouin zone. The corresponding dispersion relation is plotted in Figure 14.3 over the graphene's hexagonal Brillouin Zone (BZ) using different visualization methods.

A notable characteristic of the $E - \mathbf{k}$ relation is the presence of a conical structure at the K and K' points (vertices of the BZ where the valence and conduction bands meet). Due to this local linear relation for low-energy levels, the electrons behave as massless Dirac fermions leading to the onset of Klein tunneling (where an electron enters a potential barrier with unity transmission probability) [33]. This effect was predicted by theory for a graphene $p - n$ junction [34] and further confirmed by experiments [35].

UNCORRECTED PROOFS

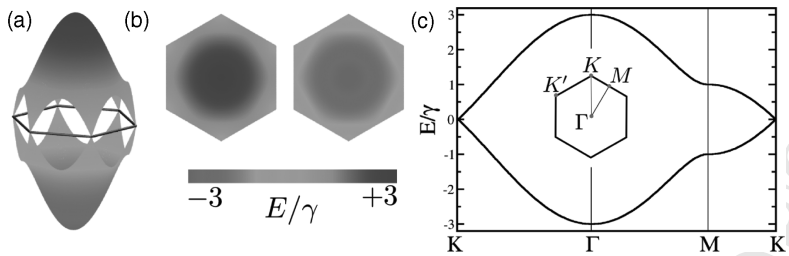

Figure 14.3 *Electronic band structure for the graphene over the Brillouin zone in a 3D (a) and 2D (b) representations and along the high symmetry lines (c). The Fermi level is at* $E = 0$

14.3.2 Graphene Nanoribbons

Graphene is regarded as a promising candidate for replacing silicon technology as silicon approaches its miniaturization limit [36]. One of the reasons for such interest in graphene is its high electronic mobility and low contact resistance [37,38]. Even though graphene itself has a rich physics, both chemical and physical modifications can be used to further tune its properties [39]. For example, ideal infinite graphene is not a semi-conducting system and the absence of an energy gap is a fundamental impediment for some applications in nanoelectronics. To remedy this issue, it is possible to modify graphene's structure to induce an opening of the energy bands around the Fermi energy. One widely studied approach is to induce quantum confinement along one in-plane direction, thus creating structures called graphene nanoribbons, which are the topic of this chapter. GNRs present electronic properties strongly dependent on their width and edge structure. For the most symmetric cases of armchair (n-AGNR, Figure 14.4 a) and zigzag (n-ZGNR, Figure 14.4 b) edged ribbons, their width is trivially obtained from the number n of $C-C$ dimer lines or zigzag strips, respectively.

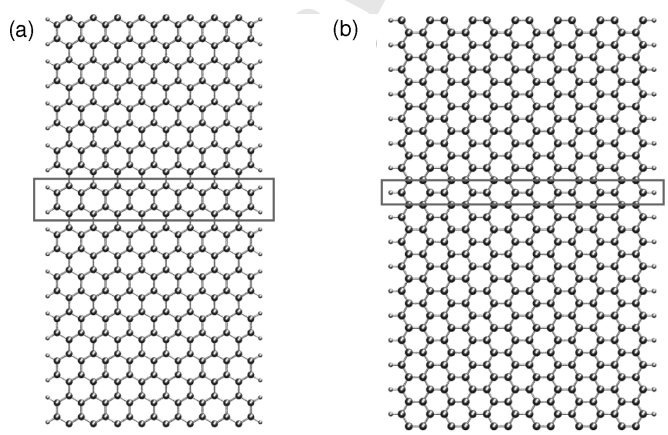

Figure 14.4 *Basic structures for AGNRs (a) and ZGNRs (b). The boxes indicate the GNRs unit cells. The periodic direction is along the vertical axis*

UNCORRECTED PROOFS

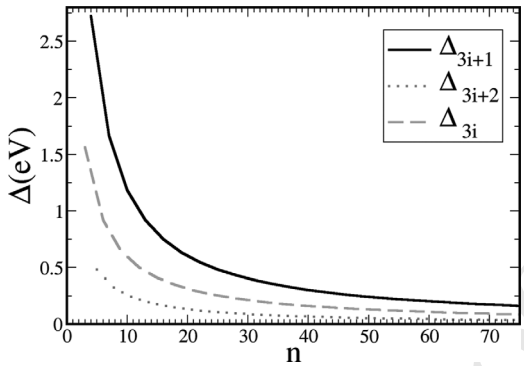

Figure 14.5 *Electronic band gap Δ for an AGNR as a function of the number n of $C-C$ lines. The three families correspond to $n = 3i + j$ with $j = 0, 1, 2$*

Theory predicts that AGNRs present a semi-conducting character with a band gap Δ_n strongly dependent on the number n of $C-C$ lines along its width. While the gap of an n-AGNR with $n \to \infty$ tends to zero (so as to recover the graphene result), the Δ_n *versus* n curve has three different branches such that $\Delta_{3i+1} \geq \Delta_{3i} \geq \Delta_{3i+2}$ [17]. In Figure 14.5 we show the calculated band gaps for various AGNR width as a function of n using the tight-binding method described in Section 14.2.

Compared to AGNRs, ZGNRs present a richer set of properties. While spin polarization is absent in AGNRs, ZGNRs possess ferromagnetically polarized edges with two possibilities for edge-to-edge polarization. These two possibilities correspond to parallel (ferromagnetic–FM) and anti-parallel (anti-ferromagnetic–AFM) alignments, the latter being the overall ground state. The spin polarization for these two states together with the non-polarized paramagnetic (PM) spin distribution are illustrated in Figure 14.6 with their corresponding band structures calculated using the TBU method.

One observes that the PM state has two two-fold degenerate bands around the Fermi energy which meet and become a flat four-fold degenerated band which extends along one third of the BZ and whose energy value approaches $E_F = 0$ as the ribbon width increases [14]. These states are strongly localized along the edges (therefore the four-fold degeneracy: two due to the spin and two due to the two symmetric edges), producing a high concentration of low energy electrons [15]. Such edge states are predicted to be responsible for a paramagnetic behavior of ZGNRs at low temperatures [40], while a diamagnetic behavior is expected at high-temperature. This high density indeed produces a instability (paramagnetic instability) which gives rise to the two lower energy magnetic states. One observes that the spin up and down polarizations along the opposite edges are located on different graphene sublattices for the AFM case which turns out to be the ground state [15]. In the FM case, edge atoms belonging to both sub-lattices present the same spin orientation and this ends up raising slightly the FM energy compared with AFM. While AFM is lower in energy, a remarkably interesting fact about these AFM and FM states is the small energy difference between them. In the upper panel of Figure 14.7 we show the TBU band-energy difference between the AFM and FM states for one ZGNR cell as a function of n. It is clear that this difference vanishes as the ribbon width increases, indicating a lowering in the edge-to-edge interaction as they are farther apart. A possible switching property based

UNCORRECTED PROOFS

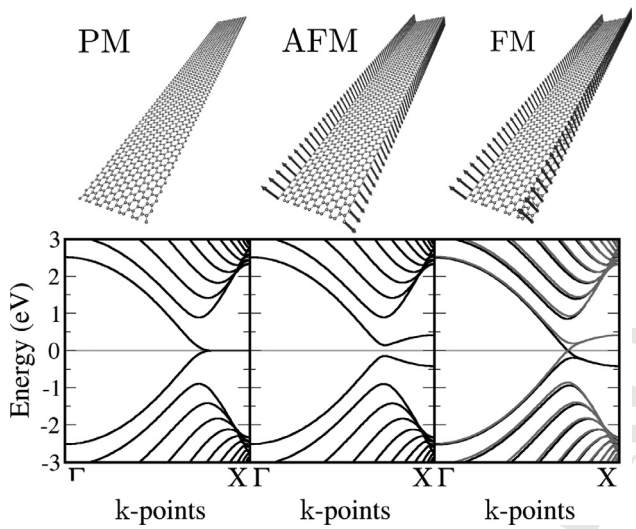

Figure 14.6 *Paramagnetic (PM), anti-ferromagnetic (AFM) and ferromagnetic (FM) states in a ZGNR and their corresponding band structures (the middle line is the Fermi energy, and curved lines are spin up and down levels)*

on this low energy difference is an interesting aspect that motivates the concept of a ZGNR based magnetic sensor [41]. These states are considerably more stable than the PM states [15]. As shown in the lower panel of Figure 14.7, this paramagnetic instability approaches its upper limit as the the ribbon's width is increased.

The existence of the rich magnetic properties opens up a number of exciting possibilities for the use of finite pieces of graphene in nanoelectronics and spintronics. For instance, it has

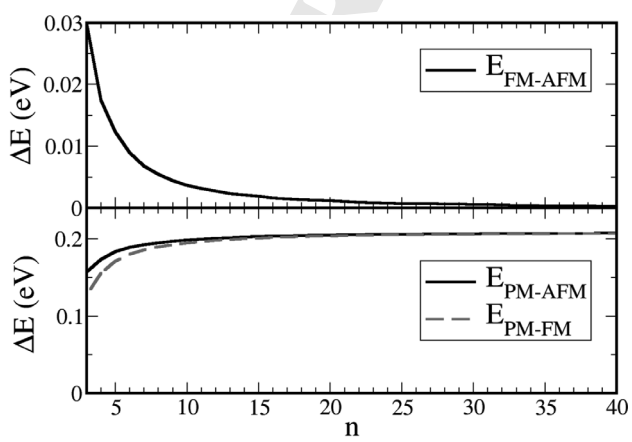

Figure 14.7 *Energy difference between any pair of different magnetic states in a ZGNR with $n = 3, \ldots, 40$. The calculation was performed using the TB band-structure energy. The difference in energy indicates that the magnetic ordering is easily destroyed at room temperature, especially for wide enough ZGNRs*

been shown that ZGNRs present a half-metallicity behavior (where the electronic structure has a metallic character for spin-up levels and is semi-conducting for spin-down levels, or vice- versa) which can be tuned using a gate voltage [16]. The importance of the details of the conductance and valence states in ZGNRs in their various spin-distributions is further demonstrated by a plot of the local current distribution using the formalism embodied by Eq. 14.8. Figure 14.8 (Plate 13) is an overview of the spin-polarized conductance at various chemical potentials for the PM, FM, and AFM states. Here, the structures are connected to perfect electrodes made of the same materials and it follows that these representations

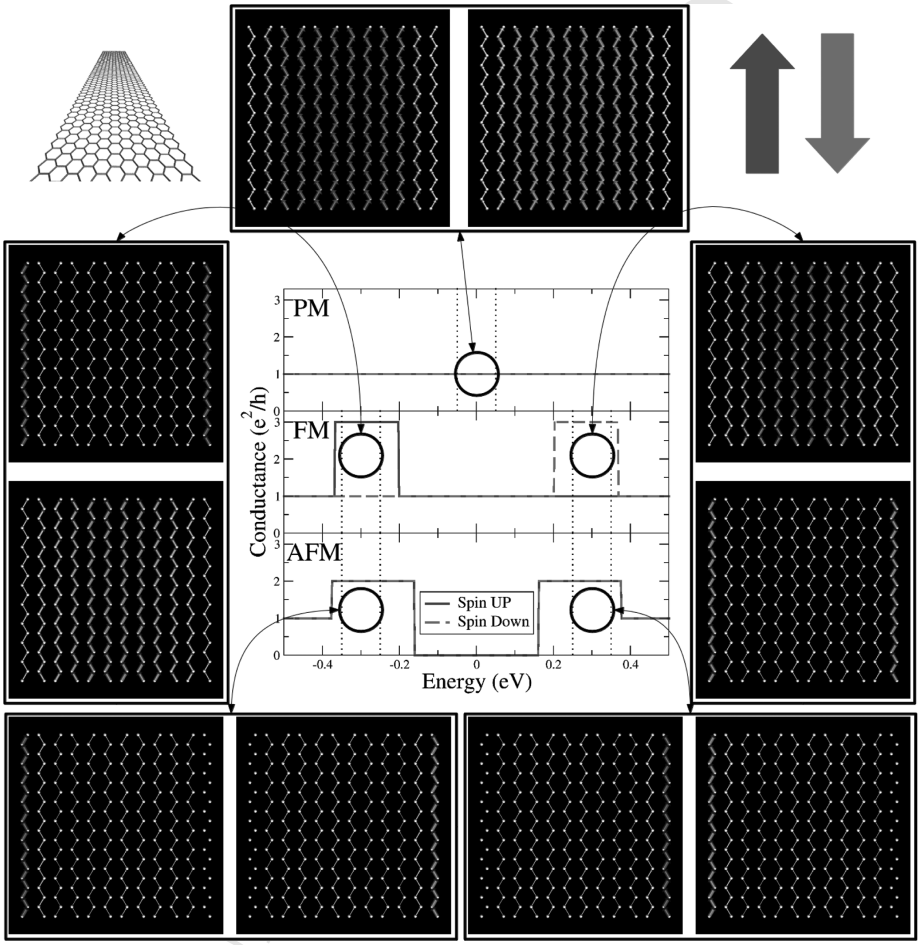

Figure 14.8 (Plate 13) *Quantum conductance as a function of energy (center) for the PM, FM and AFM states in a 12-ZGNR (full blue curves correspond to spin-up and red dashed lines to spin-down). For each state we present local current plots corresponding to* $\mu_1 = -0.35$ *eV and* $\mu_2 = -0.25$ *eV and to* $\mu_1 = +0.25$ *eV and* $\mu_2 = +0.35$ *eV for both the AFM and FM states and* $\mu_{1/2} = +/-0.05$ *eV for the PM case (chemical potential windows marked by vertical black dotted lines), both to spin-up (blue) and -down (red)*

are similar to the spatial distributions of Bloch states. For example, in the ground state (AFM), a remarkable 1D localization of the states along the edge can be seen with spin-up and spin-down channels localized at opposite sides the structure. Note that experimental evidence indicates that edges are usually made up of a mixture of armchair and zigzag edges, thereby forming what's usually referred to as *chiral* edges (see, e.g., Refs. [42, 43] and references therein).

14.4 Graphene Nanoribbon Synthesis and Processing

A large number of systems studied theoretically are often deemed unrealistic due to their narrow sizes and/or to their highly specific atomic structure. While graphene's isolation is a recent experimental achievement, the synthesis of narrow nanoribbons has also been significantly improved over the past few years. However, these accomplishments need to present additional quality for technological applications: their clean production in bulk quantity needs to be practical. In addition, large-scale deployment of GNR-based electronics calls for the possibility of packing billions of such devices onto a centimeter-wide chip wafer. Graphene pieces with well-defined size and edge structure are essential for such applications [44]. This demands a high level of control over the synthesis and manipulation of nanostructures in order to stitch them together in specific and highly ordered conformations. To address this pressing issue, a series of top-down and bottom-up approaches have been developed to obtain GNRs and other graphene like systems [37]. The former route is mainly concentrated on etching pre-synthesized graphene and lithography methods [45–47] as well as carbon nanotube unzipping [48–50]. However, in many cases, the existence of stochastic defect distributions linked to the presence of these topological irregularities in graphene prevents faithful reproducibility in the crafting process [37, 46].

At the same time, as it is difficult to create GNRs with defect free edges, it has been shown that the intriguing electronic and magnetic properties of GNRs are strongly related to clean edges. Edge defects can effectively suppress some of the most important properties of GNRs for applications [51]. Unfortunately, most GNR synthesis approaches do not allow full control over clean edge formation. Moving toward the ultimate goal of atomically sharp edges, bottom-up approaches are successful alternatives for large-scale production of GNRs. They are typically based on chemical vapor decomposition (CVD) techniques and on the assembling of complex structures by fusing small molecular building blocks [37,43,52–55]. The general strategy is to heat a gaseous solution of molecular precursors over a given substrate in order to promote growth of more complex structures. These approaches take advantage of surface assisted reactions which reduce the degrees of freedom of the molecular building blocks and can result in narrow highly crystalline systems. During this engineering process, a number of aspects have to be carefully taken into account as they can prevent the success of the synthesis protocol to obtain the desired product. The interplay between diffusion energies and surface coupling is one of these factors [37, 53, 55–57]. In addition, recent scanning tunneling microscopy images have indicated the presence of non-hexagonal rings, such as pentagons, at the edge of CVD-grown GNRs [43], while joule-heating post-synthesis approaches were shown capable of cleaning up rough structures into perfectly crystalline edged-systems [58].

UNCORRECTED PROOFS

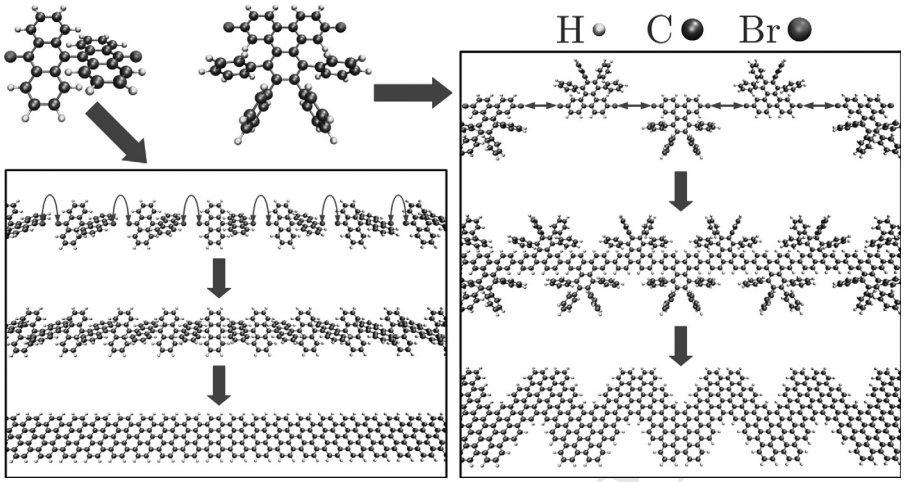

Figure 14.9 *Illustration of the bottom-up approach to obtain graphene nanoribbons with clean armchair edges and wiggle-like structures based on specific choices of the precursor monomer [54]. In the first thermally activated stage, the halogens are removed from the molecules and diffusion of the radicals over the substrate surface allows the formation of a linear polymer chain. In the following stage, a dehydrogenation process takes place, resulting in the assembly of narrow and crystalline ribbons*

The choice of the molecular precursors is a critical determining feature to be considered in such pre-programmed processes for obtaining graphitic ribbons. The experiment conducted by Cai et al., [54] is a remarkable example of this aspect. While conducting a surface-assisted pre-programmed reaction (see Figure 14.9), they showed that 10,10'-dibromo-9,9'-bianthryl molecules used as precursor yield straight and narrow crystalline carbon nanoribbons with an armchair edge geometry. In addition, starting with a 6,11-dibromo-1,2,3,4-tetraphenyltriphenylene molecule precursor, the final result is a more complex chevron-like (or wiggle-like) ribbon [54], as illustrated in Figure 14.9. This approach is also able to form other complex structures including three-terminal GNR junctions.

14.5 Tailoring GNR's Electronic Properties

Carbon based materials are sought as candidates for integrated nanoelectronics to overcome the shortcomings of silicon and to maintain the current development trends that have followed Moore's law for the past 45 years. Graphene nanoribbons are among the most promising materials for this quest, due to their unique structure-dependent electronic properties [40, 59, 60], as reviewed in Section 14.3. GNRs can be either semi-conductive or metallic, depending on their edge geometry and magnetic order [15, 17]. However, the energy gap is strongly dependent on the nanoribbon width [17]. For experimentally feasible nanoribbon widths, semiconductive GNRs have energy band-gaps on the order of a few hundredths to a few tenths of eV, which are comparable to thermal energies and are impractical for integrated nanoelectronic applications. Several methods have been explored

to increase the energy gap and modulate the electronic properties of GNRs, ranging from defect-based to chemical-based methods.

14.5.1 Defect-Based Modifications of the Electronic Properties

14.5.1.1 Non-Hexagonal Rings

Terrones and Mackay proposed that pentagon and heptagon (5–7) pairs could be introduced in planar graphitic structures without modifying the long-range planarity of the structure, as opposed to the curvature changes introduced by only pentagons or heptagons [61]. 5–7 pairs and other higher order rings, such as 5–8–5 groups, could be found as grain boundaries between graphitic domain with different orientations, and similar structures were later observed experimentally by Simonis and coworkers [62]. Koskinen et al. proposed that un-passivated zigzag edges in graphene nanoribbons could undergo a bond rotation that would change the hexagons at the zigzag edge into a sequence of pentagons and heptagons, transforming the zigzag edge into an armchair one [63]. Later, the same group reported the observation of such edges [64] from analysis of high resolution transmission electron microscope (HRTEM) images obtained by Girit et al. [65]. In a similar study, Dubois et al. later investigated the effects of pentagon and heptagon rings at the edges of armchair graphene nanoribbons, showing that defects break the aromaticity of the edge atoms and severely affect the conductance of the system [66].

Defects play an important role in the science of sp^2 carbon materials and offer an additional degree of freedom to tune their properties. Extended lines of defects (ELDs – Figure 14.13 a) and grain boundaries (GBs) are natural defects that can be found in some synthesized graphene samples and they can assume a highly crystalline organization. Both extended line defects [67] and grain boundaries [68] in graphene are predicted theoretically to have interesting electronic and transport properties stemming from the interface between systems of varying properties. These structures do not necessarily represent a problem for the goal for producing high crystalline structures, but instead open a set of new possibilities to modify and tune the properties of graphene and their GNRs to suit new applications [62, 67–71]. Botell-Mendez et al. used a chain of 5–7 pairs in order to create a seamless interface between an armchair and a zigzag nanoribbons, creating hybrid graphene nanoribbons that display new properties emerging from the presence of both zigzag and armchair edges [72]. When stitched along the periodic direction, these hybrid graphene nanoribbons display half-metallicity (Figure 14.10), as the zigzag edge presents a spin polarized edge state, while the armchair edge is non-magnetic, resulting in a spin polarized conductor. On the other hand, if stitched transverse to the periodic direction, these hybrid graphene nanoribbons have both zigzag and armchair domains, and the electronic transport across these junctions is driven by tunneling phenomena.

An even more profound example of the impact of defects in carbon nanostructures are the Haeckelite lattices (Figure 14.13 b). In these systems, an extended distribution of Stone–Wales defects is introduced over the graphene sheet so as to produce a perfectly threefold coordinated flat structures without any hexagons [73]. Even though experimental realization of these structures is still lacking, they present a set of new properties that can be further expanded, in particular in their tubular [73] and nanoribbon versions. The existence of such exciting properties motivates future experimental studies aimed at their synthesis.

UNCORRECTED PROOFS

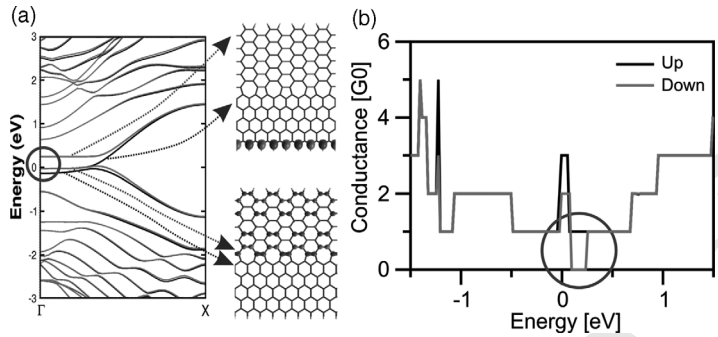

Figure 14.10 *(a) Band structure of a hybrid graphene nanoribbon with both zigzag and armchair edges. The arrows point to the wave-function plot of the states around the Fermi energy, displaying the edge state associated to the zigzag edge. (b) Electronic transport plot for this nanoribbon, revealing that the nanoribbon can be used as a spin filter on an energy window just above the Fermi energy*

14.5.1.2 Edge and Bulk Disorder

In order to provide accurate estimates of the stability of GNR-based electronic devices, an accurate account of the defects and their effects on transport properties must be taken, as these are inherent to any large scale production system. Several groups have studied the effects of edge and bulk disorder on the transport properties of graphene nanoribbons [74–79]. Specifically, Areshkin et al. used a recursive model to remove edge atoms to create vacancies at the edges that span several layers of atoms [74]. They also found that zigzag edged GNRs are more resistant to edge degradation than their armchair counterparts. While the zigzag edge is able to withstand large (50%) edge defect concentrations up to four edge layers deep, in the armchair case only a 10% erosion of the outer edge layer led to suppression of electronic transport.

Furthermore, two similar works used a GNR model with a random edge disorder for widths similar to experimentally available devices [75, 78, 80]. They found that even moderate edge roughness is enough to cause localized scattering centers leading to Anderson localization and creating an electron transport gap, in accordance with the experimental results [80].

Finally, note that atomic vacancies have also been proposed to modify local properties [81], resulting in an enhancement of the system's reactivity and opening a set of new possibilities for the physics and chemistry of these structures.

14.5.2 Electronic Properties of Chemically Doped Graphene Nanoribbons

14.5.2.1 Substitutional Doping of Graphene Nanoribbons

Substitutional doping by non-carbon atoms has been widely studied as a method for tailoring the electronic properties of other carbon-based materials such as fullerenes and carbon nanotubes. The rationale behind this interest is that ions of atoms with similar size to carbon (boron and nitrogen, in particular) could be easily inserted into the graphitic hexagonal lattice. In addition, it was earlier found that boron and nitrogen could respectively introduce acceptor or donor states in carbon nanotubes [82]. Substitutional doping of graphene has

UNCORRECTED PROOFS

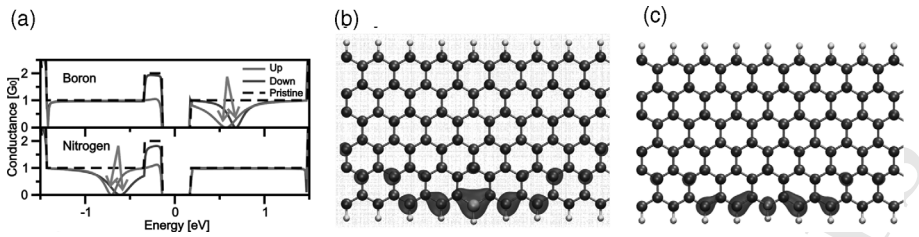

Figure 14.11 *(a) Electronic transport of boron and nitrogen doped graphene nanoribbons. The arrows indicate the donor-like (boron) and acceptor-like (nitrogen) states. Local density of states (LDOS) plots for the nitrogen (b) and boron (c) localized states at the energies indicated by the arrows on the plot (a)*

been experimentally achieved by different methods, such as electrothermal reactions [83], hydrocarbon pyrolysis in presence of ammonia [84], and arc discharge [85], among others.

A number of theoretical studies of the effect of substitutional doping on graphene nanoribbons electronic transport have been carried out by several groups. One of the earliest studies of such effects were carried by Martins and coworkers who focused on doped narrow graphene nanoribbons, finding that introduction of doping atoms that interact with the carbon π states creates a spin anisotropy in the electronic transport around the energy corresponding to the localized state near the dopant [86, 87]. It was proposed that substitutional doping could be used to create graphene-based spin polarized conductors. Other works also focused on the effects of boron and nitrogen doping on wider graphene nanoribbons [88, 89], while Cruz-Silva also examined the effects of substitutional doping with phosphorus on GNRs [90]. A surprising effect of doping found in these cases is that for zigzag GNRs, both nitrogen and boron could induce donor or acceptor states depending on their position within the nanoribbon. As observed in Figure 14.11, the energies of the localized states created by the doping atoms change as their position in the nanoribbon is closer to the edges, until finally crossing over the Fermi energy and moving to the other side of the energy spectrum. This effect can be explained by the increased exchange interaction due to the localization of the dopant-induced states and the zigzag edge states [90].

14.5.2.2 Chemical Functionalization of Graphene Nanoribbons

A different pathway for modifying the electronic and transport properties of graphene nanoribbons is through the use of chemical functionalization. As mentioned before, modifications of the carbon π network, by doping or chemical interactions, result in changes of the electronic structure near the Fermi energy. Such changes allow tailoring of the electronic transport properties at low voltages [87]. There are a variety of techniques to enable functionalization of graphene such as hydrogenation [91, 92], oxidation [93–95], and chemical attachment of metallic atoms [96].

Fully hydrogenated graphene (graphane) was first theoretically proposed by Sofo et al. [97], and experimentally achieved by Elias et al. [91]. On an sp^2 carbon atom, hydrogen can only bond to the free π_z orbital, forcing a change to an sp^3 hybridization on the host atom and forming a σ bond. Since full hydrogenation of graphene results in the rehybridization of all carbon atoms, graphane can be thought of as a single diamond layer, and is a wide gap semiconductor (as is diamond).

UNCORRECTED PROOF

Selective hydrogenation, however, can be used to modify the electronic properties of graphene nanoribbons. An example of this is the study by Soriano et al. [92], where the authors used both DFT and TBU to study the tunneling magnetoresistance of a doubly hydrogenated armchair GNR as a function of the distance between hydrogenated sites. They found that hydrogenation of sites close to the nanoribbon edges are more energetically stable than those occuring within the central atoms. They also found that the near-edge hydrogenation is more effective at creating a tunneling magnetoresistance, and propose that this kind of hydrogenated nanoribbons has potential use in spintronic applications [92].

Oxygen, as well as other functional groups that attach to sp^2-based carbon nanostructures, can modify the $\pi-$ orbital network. It was shown early on that by attaching oxygen, hydroxyl (OH), or imine (NH) groups at the edges of a zigzag GNR, it could be possible to indirectly close the energy gap in the antiferromagnetic ground state of zigzag GNRs [93]. Using localized Wannier functions, Cantele et al. showed that the states induced by oxygen at the Fermi energy are due to lone pair states [95]. Another approach to study the effects of oxidation is based a decimation method to perform quantum transport calculations on real-length graphene nanoribbons (up to 600 nm) [94]. They found that the elastic mean free path for these nanoribbons strongly decays with increasing number of hydrogen and hydroxyl functional groups attached to the nanoribbon. Other attempts to modify the electronic structure of GNRs are based on connecting third row transition metal atoms to manipulate the electronic transport properties of GNRs [96, 98].

14.5.3 GNR Assemblies

14.5.3.1 Nanowiggles

It has been pointed out that systems such as the segmented structure obtained using a surface-assisted bottom-up approach can be viewed as an example of a more general set of structures called graphitic nanowiggles (GNWs) [11], since they present, in general, a wiggly edge conformation. Such GNWs can be viewed as a successive repetition of GNR sectors which can be either armchair (A) or zigzag (Z) edged (resulting in the four achiral GNW classes illustrated in Figure 14.12). Their electronic structure [11, 99] and thermoelectric transport properties [100, 101] have been studied using an array of

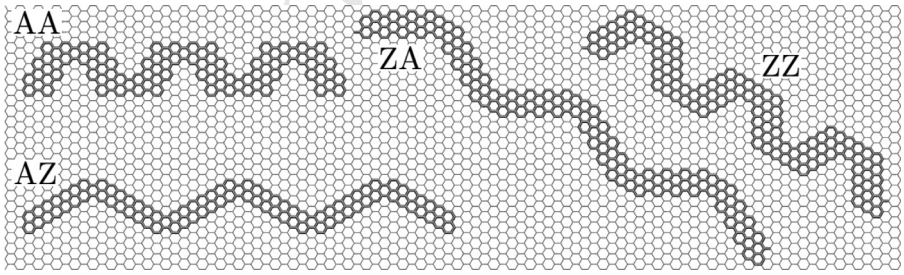

Figure 14.12 *The four classes of achiral GNWs: AA, AZ, ZA and ZZ, depending on when the parallel and oblique sectors, respectively, present either an armchair (A) or zigzag (Z) edge. The figure represents three unit cells from each case and we highlight the central one by using black atoms*

UNCORRECTED PROOFS

computational approaches. Regarding their electronic structure, GNWs with at least one zigzag sector present a set of multiple magnetic states with a rather larger diversity compared to the corresponding set from ZGNRs. Further, depending on how individual sectors are arranged together, they can present a large, quasi-continuous, range of band-gaps [11].

14.5.3.2 Antidots and Junctions

In addition to GNWs, graphene and GNRs have been assembled into several new structures. Porous systems like graphene antidot lattices, for instance, have been shown to allow a controlled manipulation of graphene's electronic properties [102] as well as on carbon nanoribbons [103, 104]. Other proposals exploit the interplay between armchair and zigzag edges in more complex ribbon geometries to demonstrate spin-filter devices and geometry-dependent controlling approaches for the localization of magnetic edge-states [105–110]. Junctions composed of A- and ZGNRs [111] and 1D GNR-superlattices [108, 109] (Figure 14.13 d) are also new structures suitable for embedding in new electronic nanodevices.

14.5.3.3 GNR Rings

While GNR-made nanorings are expected to be more stable than carbon nanotube-based tori, these systems impose boundary conditions on the electronic states, resulting in

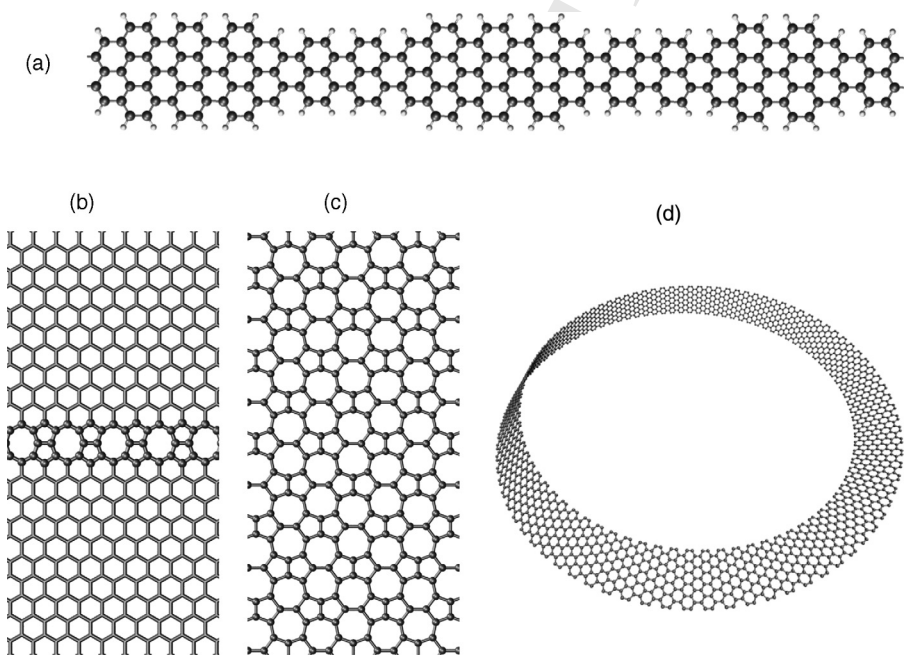

Figure 14.13 *Atomic models for the assembling of graphene and GNRs into new structures: (a) 1D GNR-based superlattice; (b) extended line of defects; (c) Haeckelite lattice; (d) Möbius-like GNR nanoring*

TED PROOFS

fascinating transport properties which include energy selectivity rules for the electronic paths on the structure [112]. In a separate theoretical prediction, Möbius rings (Figure 14.13 c) have been predicted to present specific UV/vis spectra signatures [113] and characteristic charge localization due to curvature [114].

14.5.3.4 GNR Stacking

The stacking of multiple GNRs is predicted to have a major influence on the electronic structure and magnetic states of these multi-layer systems due to an interplay between intralayer and interlayer coupling [115]. On the other hand, the behavior of the electronic current as a function of temperature and device length is now well understood in terms of *ab initio* calculations [116]. Note also that the stacking of two GNRs bound by van der Waals forces can be used as a rheostat with cross-GNR conductance being finely tuned by the relative angle between the two GNRS [111]. In this case, multi-terminal transport formalism must be employed (Eq. 16.6) to evaluate electronic transmission between any two sides of one layer and the corresponding ones of the second layer.

14.6 Thermoelectric Properties of Graphene-Based Materials

14.6.1 Thermoelectricity

The thermoelectric effect is the direct conversion between temperature gradients and voltage differences, and can be used in energy conversion like power generation and cooling applications such as refrigeration [117, 118]. Ideal thermoelectric materials are required to have good electric conduction yet poor heat conduction and their thermoelectric conversion efficiency is indicated by the dimensionless figure of merit $ZT = S^2GT/k$, where S is thermal power (or Seebeck coefficient), T is average temperature, G is electrical conductance and k is total thermal conductance $k = k_{el} + k_{ph}$ (including contributions from electrons k_{el} and phonons k_{ph}). Devices with $ZT > 1$ are usually considered good thermoelectrics, but $ZT > 3$ is often regarded as a minimal requirement for competing with conventional generators and refrigerators [118]. For this reason, considerable attention has been devoted toward the discovery or design of materials with enhanced ZT. This can be realized by two approaches. One method is to increase the Seebeck coefficient S by reducing the dimensionality of the system [119, 120]. The other idea is to suppress phonon thermal conductance k_{ph} together with a sharp resonance in the electronic conductance G [121, 122], which has been the focus of experimental and theoretical efforts.

14.6.2 Thermoelectricity in Carbon

Graphene has also attracted interest due to its outstanding thermal properties. A huge Seebeck coefficient (30 mV/K) has been predicted for graphene gated by a sequence of metal electrodes [123] while a superior thermal conductivity as high as 5 kW/mK has been measured [124, 125]. However, the extremely high thermal conductance means that graphene is not intrinsically a good thermoelectric device. Strategies are needed to degrade its thermal conductance while preserving or enhancing the high electronic conductance and thermopower characteristics. Several enabling routes have already been examined, such

UNCORRECTED PROOFS

as the use of isotopes [126], strain [127], edge passivation [128, 129], random hydrogen vacancies [130], atomic vacancies and defects [120, 131, 132], molecular junctions [121, 133], multi-juctions GNRs and superlattices [100, 101, 122, 132], and edge disorder [134].

It was discovered that AGNRs show lower thermal conductance than ZGNRs of similar width, suggesting that AGNRs are better candidates to be optimized for thermoelectric performance [100, 129]. However, peak ZT values for pristine AGNRs at room temperature are far less than 1. Theoretical calculations by Chen et al. [100] indicate that peak ZT value for the narrowest AGNR is less than 0.4 and it generally decreases with a width increase. Atomic vacancies and Stone–Wales defects have been introduced to suppress phonon thermal conductance. A 0.23% double vacancy or Stone–Wales concentration leads to a 80% reduction in thermal conductance of GNRs from pristine ones [131]. However, corresponding ZT values at room temperature are not significantly enhanced (less than 0.5) due to the concomitant reduction of the electrical conductance [132] reported that the reduction of phonon thermal conductance by random vacancies can be fully compensated by the concomitant reduction of electrical conductance, which results in a reduction of ZT compared to perfect AGNRs. However, a periodic distribution of vacancies inside the ribbon may be seen as a reduction of the effective width, which tends to reduce the thermal conductance while enhancing the thermopower, leading to higher ZT. Additionally, multi-junctions GNRs have been proposed to degrade phonon thermal conductance [100, 101, 122]. A specific patterning of a mixed GNR obtained by alternating armchair and zigzag sections of different widths has been shown to provide high thermoelectric performance with a ZT factor reaching unity at room temperature (Figure 14.14) [122]. Besides the reduction of phonon thermal conductance, the resonant tunneling of electrons between these sections retains high electron conductance and Seebeck coefficient. Finally, the introduction of edge disorder has been predicted to dramatically reduce phonon thermal transport while only weakly decreasing electronic conduction [134], resulting in ZT higher than 1 at room temperature in the diffusive limit (Figure 14.15).

Although theoretical calculations indicate that GNRs can be modified to have good thermoelectric performance, those modifications are experimentally challenging. The newly

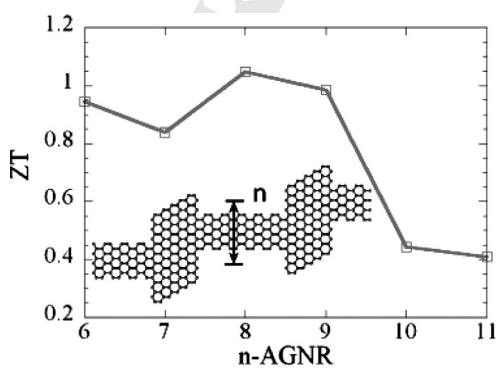

Figure 14.14 *Maximum ZT value as a function of the number of dimers n in armchair sections in the multijuction structure [122]. Reprinted with permission from Ref. [22] Copyright 2011 the American Physical Society*

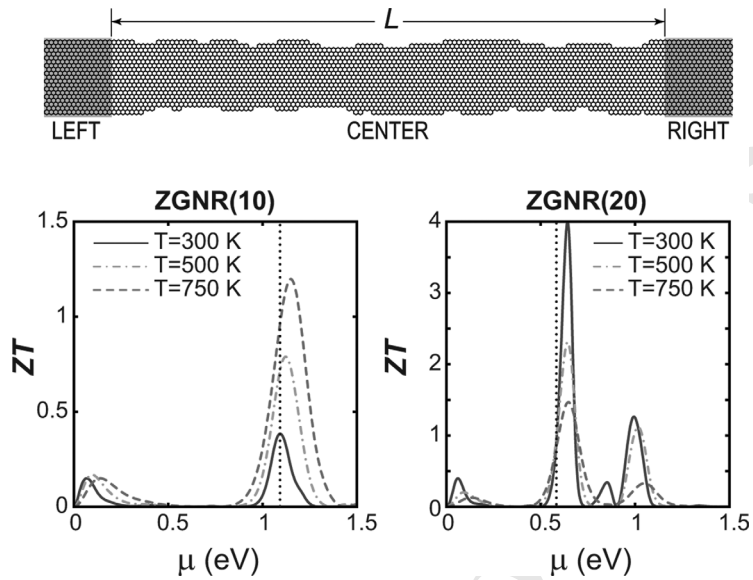

Figure 14.15 *Thermoelectric properties in edge-disordered GNR. The central region with edge disorder has length L and is connected to semi-infinite ZGNRs free of disorder. Thermoelectric figure of merit, ZT, versus chemical potential μ at different temperatures T for ZGNR10 and ZGNR20 having lengths L = 0.25 nm and 4 μm, respectively [134]. Reprinted with permission from Ref. [134] © 2010 the American Physical Society*

synthesized wiggle-type GNRs, so called graphitic nanowiggles (see Section 14.5.3 and Figure 14.12), have been fabricated with an atomically precise bottom-up approach using surface-assisted coupling of molecular precursors into linear polyphenylenes. Their intrinsic electronic and magnetic properties have been demonstrated for a number of arrangements and edge symmetries [11]. The attractiveness of these structure is their high-order (making them good electronic conductors) with regularly repeated junctions between different domain (making them poor thermal conductors). The wiggle edges reduce phonon thermal conductance by nearly 50% and double peak ZT values in comparison to straight GNRs of similar width [100], demonstrating GNWs as promising thermoelectric materials. Note also that a recent computational investigation showed that ZT can be optimized up a value of 5 by drilling nanopores into the GNRs: the holes effectively suppress phonon transport without significantly affecting the electron transport since it essentially flows along the edges of ZGNRs [135].

14.7 Conclusions

Modern theoretical and computational science provide opportunities to explore fundamental physics and chemistry at the length and time scales where the materials properties and behavior are controlled and is thereby a key to performing predictive design. When integrated with experimental studies at the same time and length scales, validated discoveries

UNCORRECTED

JWST348-c14 JWST348-Jiang May 31, 2013 11:34 Printer Name: Markono Trim: 244mm × 170mm

are possible and enable novel discoveries and potential breakthroughs in areas such as nanoelectronics. In this chapter we have reviewed recent research in the area of electronic transport of GNRs and GNR assemblies. Electron transport in GNRs is a rapidly moving field and the present review is not an attempt to be exhaustive. Instead, we have presented an overview of the major research directions that can provide a viable pathway towards the fine-tuning of the properties of GNR systems for future applications in nano electronics optoelectronics and spintronics.

Acknowledgements

ECG acknowledges support from Brazilian agencies CAPES (process 0327-10-7) and CNPq (process 140887/2008-3). ECS was supported in part by PHASE, an EFRC funded by the US-DOE under Award Number DE-SC0001087. VM and BGS acknowledge support from the Center for Nanophase Materials Sciences (CNMS), sponsored at ORNL by the Scientific User Facilities Division, Office of Basic Energy Sciences, U.S. DOE. VM is also supported by New York State under NYSTAR contract C080117. Some of the original computations used resources of the Oak Ridge Leadership Computing Facility and the NCCS.

References

[1] Kroto HW, Heath JR, Obrien SC, Curl RF, Smalley RE. C-60 – Buckminsterfullerene. *Nature*. 1985;318(6042):162–163.
[2] Iijima S. Helical microtubules of graphitic carbon. *Nature*. 1991;354(6348):56–58.
[3] Novoselov K, Geim A, Morozov S, Jiang D, Zhang Y, Dubonos S, et al. Electric field effect in atomically thin carbon films. *Science*. 2004;306(5696):666–669.
[4] Sumpter BG, Meunier V. Can computational approaches aid in untangling the inherent complexity of practical organic photovoltaic systems? *Journal of Polymer Science Part B: Polymer Physics*. 2012.
[5] Milnera M, Kürti J, Hulman M, Kuzmany H. periodic resonance excitation and intertube interaction from quasicontinuous distributed helicities in single-wall carbon nanotubes. *Physical Review Letters*. 2000;84(6):1324–1327.
[6] Saito R, Dresselhaus G, Dresselhaus MS. Trigonal warping effect of carbon nanotubes. *Physical Review B.* 2000;61(4):2981–2990.
[7] Reich S, Maultzsch J, Thomsen C, Ordejón P. Tight-binding description of graphene. *Physical Review B.* 2002;66:035412.
[8] Gunlycke D, White CT. Tight-binding energy dispersions of armchair-edge graphene nanostrips. *Physical Review B.* 2008;77:115116.
[9] Girão EC, Souza Filho AG, Meunier V. Electronic transport properties of carbon nanotoroids. *Nanotechnology.* 2011;22(7):075701.
[10] Saito R, Dresselhaus G, Dresselhaus MS. *Physical Properties of Carbon Nanotubes.* London: Imperial College Press; 1998.
[11] Girão EC, Liang L, Cruz-Silva E, Souza Filho AG, Meunier V. Emergence of atypical properties in assembled graphene nanoribbons. *Physical Review Letters.* 2011;107:135501.

UNCORRECTED PROOFS

[12] Yazyev OV. Hyperfine interactions in graphene and related carbon nanostructures. *Nano Letters.* 2008;8(4):1011–1015.
[13] Fischer J, Trauzettel B, Loss D. Hyperfine interaction and electron-spin decoherence in graphene and carbon nanotube quantum dots. *Physical Review B.* 2009;80:155401.
[14] Yazyev OV. Emergence of magnetism in graphene materials and nanostructures. *Reports on Progress in Physics.* 2010;73(5):056501.
[15] Pisani L, Chan JA, Montanari B, Harrison NM. Electronic structure and magnetic properties of graphitic ribbons. *Physical Review B.* 2007;75(6):064418.
[16] Son YW, Cohen ML, Louie SG. Half-metallic graphene nanoribbons. *Nature.* 2006;444(7117):347–349.
[17] Son YW, Cohen ML, Louie SG. Energy gaps in graphene nanoribbons. *Physical Review Letters.* 2006;97(21):216803.
[18] Hod O, Peralta JE, Scuseria GE. Edge effects in finite elongated graphene nanoribbons. *Physical Review B.* 2007;76:233401.
[19] Hod O, Barone V, Scuseria GE. Half-metallic graphene nanodots: A comprehensive first-principles theoretical study. *Physical Review B.* 2008;77:035411.
[20] Jiang D, Dai S. Circumacenes versus periacenes: HOMO-LUMO gap and transition from nonmagnetic to magnetic ground state with size. *Chemical Physics Letters.* 2008;466(1–3):7275.
[21] Fernández-Rossier J, Palacios JJ. Magnetism in graphene nanoislands. *Physical Review Letters.* 2007;99:177204.
[22] Lieb EH. Two theorems on the Hubbard model. *Physical Review Letters.* 1989;62:1201–1204.
[23] Palacios JJ, Fernández-Rossier J, Brey L. Vacancy-induced magnetism in graphene and graphene ribbons. *Physical Review B.* 2008;77:195428.
[24] Fernández-Rossier J. Prediction of hidden multiferroic order in graphene zigzag ribbons. *Physical Review B.* 2008;77:075430.
[25] Ferrier M, Angers L, Rowe ACH, Guéron S, Bouchiat H, Texier C, et al. Direct measurement of the phase-coherence length in a GaAs/GaAlAs square network. *Physical Review Letters.* 2004;93:246804.
[26] Miao F, Wijeratne S, Zhang Y, Coskun UC, Bao W, Lau CN. Phase-coherent transport in graphene quantum billiards. *Science.* 2007;317(5844):1530–1533.
[27] Di Ventra M. *Electrical Transport in Nanoscale Systems.* Cambridge University Press; 2008.
[28] Datta S. *Quantum Transport: Atom to Transistor.* Cambridge University Press; 2005.
[29] Lopez-Sancho MP, Lopez-Sancho JM, Rubio J. Highly convergent schemes for the calculation of bulk and surface Green-Functions. *Journal of Physics F: Metal Physics.* 1985;15(4):851–858.
[30] Sancho MPL, Sancho JML, Rubio J. Quick iterative scheme for the calculation of transfer-matrices – application to Mo(100). *Journal of Physics F - Metal Physics.* 1984;14(5):1205–1215.
[31] Caroli C, Combesco R, Nozieres P, Saintjam D. Direct calculation of tunneling current. *Journal of Physics Part C Solid State Physics.* 1971;4(8):916.
[32] Kazymyrenko K, Waintal X. Knitting algorithm for calculating Green functions in quantum systems. *Physical Review B.* 2008;77(11):115119.

UNCORRECTED PROOFS

[33] Das Sarma S, Adam S, Hwang EH, Rossi E. Electronic transport in two-dimensional graphene. *Reviews of Modern Physics.* 2011;83(2):407–470.
[34] Cheianov VV, Fal'ko VI. Selective transmission of Dirac electrons and ballistic magnetoresistance of *np* junctions in graphene. *Physical Review Letters*. 2006 Jul;74:041403.
[35] Huard B, Sulpizio JA, Stander N, Todd K, Yang B, Goldhaber-Gordon D. Transport measurements across a tunable potential barrier in graphene. *Physical Review Letters.* 2007;98(23):236803.
[36] Schwierz F. Graphene transistors. *Nature Nanotechnology.* 2010;5(7):487–496.
[37] Palma CA, Samori P. Blueprinting macromolecular electronics. *Nature Chemistry.* 2011;3(6):431–436.
[38] Xia F, Perebeinos V, Lin Ym, Wu Y, Avouris P. The origins and limits of metal-graphene junction resistance. *Nature Nanotechnology.* 2011;6(3):179–184.
[39] Novoselov K. Mind the gap. *Nature Materials.* 2007;6(10):720–721.
[40] Wakabayashi K, Fujita M, Ajiki H, Sigrist M. Electronic and magnetic properties of nanographite ribbons. *Physical Review B.* 1999;59(12):8271–8282.
[41] Munoz-Rojas F, Fernandez-Rossier J, Palacios JJ. Giant Magnetoresistance in Ultra-small Graphene Based Devices. *Physical Review Letters.* 2009;102(13):136810.
[42] Tao C, Jiao L, Yazyev OV, Chen YC, Feng J, Zhang X, et al. Spatially resolving edge states of chiral graphene nanoribbons. *Nature Physics.* 2011 AUG;7(8):616–620.
[43] Pan M, Girão EC, Jia X, Bhaviripudi S, Li Q, Kong J, et al. Topographic and spectroscopic characterization of electronic edge states in CVD grown graphene nanoribbons. *Nano Letters.* 2012;12(4):1928.
[44] Barone V, Hod O, Scuseria GE. Electronic structure and stability of semiconducting graphene nanoribbons. *Nano Letters.* 2006;6(12):2748–2754.
[45] Wang X, Dai H. Etching and narrowing of graphene from the edges. *Nature Chemistry.* 2010;2(8):661–665.
[46] Yang R, Zhang L, Wang Y, Shi Z, Shi D, Gao H, et al. An anisotropic etching effect in the graphene basal plane. *Advanced Materials.* 2010;22(36):4014–4019.
[47] Xie L, Jiao L, Dai H. Selective etching of graphene edges by hydrogen plasma. *Journal of the American Chemical Society.* 2010;132(42):14751–14753.
[48] Kosynkin DV, Higginbotham AL, Sinitskii A, Lomeda JR, Dimiev A, Price BK, et al. Longitudinal unzipping of carbon nanotubes to form graphene nanoribbons. *Nature.* 2009;458(7240):872.
[49] Jiao L, Zhang L, Wang X, Diankov G, Dai H. Narrow graphene nanoribbons from carbon nanotubes. *Nature.* 2009;458(7240):877–880.
[50] Morelos-Gomez A, Vega-Diaz SM, Gonzalez VJ, Tristan Lopez F, Cruz-Silva R, Fujisawa K, et al. Clean nanotube unzipping by abrupt thermal expansion of molecular nitrogen: graphene nanoribbons with atomically smooth edges. *ACS Nano.* 2012;6(3):2261–2272.
[51] Jia X, Campos-Delgado J, Terrones M, Meunier V, Dresselhaus MS. Graphene edges: a review of their fabrication and characterization. *Nanoscale.* 2011;3(1):86–95.
[52] Campos-Delgado J, Romo-Herrera JM, Jia X, Cullen DA, Muramatsu H, Kim YA, et al. Bulk production of a new form of sp2 carbon: crystalline graphene nanoribbons. *Nano Letters.* 2008;8(9):2773–2778.

UNCORRECTED PROOFS

[53] Grill L, Dyer M, Lafferentz L, Persson M, Peters MV, Hecht S. Nano-architectures by covalent assembly of molecular building blocks. *Nature Nanotechnology.* 2007;2(11):687–691.
[54] Cai J, Ruffieux P, Jaafar R, Bieri M, Braun T, Blankenburg S, et al. Atomically precise bottom-up fabrication of graphene nanoribbons. *Nature.* 2010;466(7305):470–473.
[55] Bieri M, Nguyen MT, Groening O, Cai J, Treier M, Ait-Mansour K, et al. Two-dimensional polymer formation on surfaces: insight into the roles of precursor mobility and reactivity. *Journal of the American Chemical Society.* 2010;132(46):16669–16676.
[56] Lu J, Yeo PSE, Gan CK, Wu P, Loh KP. Transforming C_60 molecules into graphene quantum dots. *Nature Nanotechnology.* 2011;6(4):247–252.
[57] Lafferentz L, Ample F, Yu H, Hecht S, Joachim C, Grill L. Conductance of a single conjugated polymer as a continuous function of its length. *Science*. 2009;323(5918):1193–1197.
[58] Jia X, Hofmann M, Meunier V, Sumpter BG, Campos-Delgado J, Romo-Herrera JM, et al. Controlled formation of sharp zigzag and armchair edges in graphitic nanoribbons. *Science.* 2009;323(5922):1701–1705.
[59] Castro Neto AH, Guinea F, Peres NMR, Novoselov KS, Geim AK. The electronic properties of graphene. *Rev Mod Phys.* 2009 Jan;81:109–162.
[60] Nakada K, Fujita M, Dresselhaus G, Dresselhaus MS. Edge state in graphene ribbons: Nanometer size effect and edge shape dependence. *Phys Rev B.* 1996 Dec;54:17954–17961.
[61] Terrones H, Mackay AL. The geometry of hypothetical curved graphite structures. *Carbon.* 1992;30(8):1251–1260.
[62] Simonis P, Goffaux C, Thiry P, Biro L, Lambin P, Meunier V. STM study of a grain boundary in graphite. Surface Science. 2002;511(1-3):319–322.
[63] Koskinen P, Malola S, Häkkinen H. Self-passivating edge reconstructions of graphene. *Phys Rev Lett.* 2008 Sep;101:115502.
[64] Koskinen P, Malola S, Häkkinen H. Evidence for graphene edges beyond zigzag and armchair. *Phys Rev B.* 2009 Aug;80:073401.
[65] Girit ÇÖ, Meyer JC, Erni R, Rossell MD, Kisielowski C, Yang L, et al. Graphene at the edge: stability and dynamics. *Science.* 2009;323(5922):1705–1708.
[66] Dubois SM, Lopez-Bezanilla A, Cresti A, Triozon F, Biel B, Charlier J, et al. Quantum transport in graphene nanoribbons: effects of edge reconstruction and chemical reactivity. *ACS Nano.* 2010;4(4):1971–1976.
[67] Botello-Mendez AR, Declerck X, Terrones M, Terrones H, Charlier JC. One-dimensional extended lines of divacancy defects in graphene. *Nanoscale.* 2011;3(7):2868–2872.
[68] Yazyev OV, Louie SG. Electronic transport in polycrystalline graphene. *Nature Materials.* 2010;9(10):806.
[69] Lahiri J, Lin Y, Bozkurt P, Oleynik II, Batzill M. An extended defect in graphene as a metallic wire. *Nature Nanotechnology.* 2010;5(5):326–329.
[70] Lin X, Ni J. Half-metallicity in graphene nanoribbons with topological line defects. *Physical Review B.* 2011;84(7):075461.
[71] Ajayan PM, Yakobson BI. Graphene: Pushing the boundaries. *Nature Materials.* 2011;10(6):415–417.

UNCORRECTED PROOFS

[72] Botello-Mendez AR, Cruz-Silva E, Lopez-Urias F, Sumpter BG, Meunier V, Terrones M, et al. Spin polarized conductance in hybrid graphene nanoribbons using 5-7 defects. *ACS Nano.* 2009;3(11):3606–3612.

[73] Terrones H, Terrones M, Hernandez E, Grobert N, Charlier J, Ajayan P. New metallic allotropes of planar and tubular carbon. *Physical Review Letters.* 2000;84(8):1716–1719.

[74] Areshkin DA, Gunlycke D, White CT. Ballistic transport in graphene nanostrips in the presence of disorder: importance of edge effects. *Nano Letters.* 2007;7(1):204–210.

[75] Evaldsson M, Zozoulenko IV, Xu HY, Heinzel T. Edge-disorder-induced Anderson localization and conduction gap in graphene nanoribbons. *Physical Review B.* 2008;78(16):161407.

[76] Li TC, Lu SP. Quantum conductance of graphene nanoribbons with edge defects. *Physical Review B.* 2008;77(8):085408.

[77] Lherbier A, Biel B, Niquet YM, Roche S. Transport length scales in disordered graphene-based materials: Strong localization regimes and dimensionality effects. *Physical Review Letters.* 2008;100(3):036803.

[78] Mucciolo ER, Neto AHC, Lewenkopf CH. Conductance quantization and transport gaps in disordered graphene nanoribbons. *Physical Review B.* 2009;79(7):075407.

[79] Cresti A, Roche S. Range and correlation effects in edge disordered graphene nanoribbons. *New Journal of Physics.* 2009;11:095004.

[80] Han MY, Ozyilmaz B, Zhang YB, Kim P. Energy band-gap engineering of graphene nanoribbons. *Physical Review Letters.* 2007;98(20):206805.

[81] Amorim RG, Fazzio A, Antonelli A, Novaes FD, da Silva AJR. Divacancies in graphene and carbon nanotubes. *Nano Letters.* 2007;7(8):2459–2462.

[82] Choi HJ, Ihm J, Louie SG, Cohen ML. Defects, quasibound states, and quantum conductance in metallic carbon nanotubes. *Physical Review Letters.* 2000;84(13):2917–2920.

[83] Wang X, Li X, Zhang L, Yoon Y, Weber PK, Wang H, et al. N-doping of graphene through electrothermal reactions with ammonia. *Science.* 2009;324(5928):768–771.

[84] Qu L, Liu Y, Baek JB, Dai L. Nitrogen-doped graphene as efficient metal-free electrocatalyst for oxygen reduction in fuel cells. *ACS Nano.* 2010;4(3):1321–1326.

[85] Subrahmanyam KS, Panchakarla LS, Govindaraj A, Rao CNR. Simple method of preparing graphene flakes by an arc-discharge method. *The Journal of Physical Chemistry C.* 2009;113(11):4257–4259.

[86] Martins TB, Miwa RH, da Silva AJR, Fazzio A. Electronic and transport properties of boron-doped graphene nanoribbons. *Physical Review Letters.* 2007;98(19):196803.

[87] Martins TB, da Silva AJR, Miwa RH, Fazzio A. σ- and π-Defects at graphene nanoribbon edges: building spin filters. *Nano Letters.* 2008;8(8):2293–2298.

[88] Biel B, Blase X, Triozon F, Roche S. Anomalous doping effects on charge transport in graphene nanoribbons. *Phys Rev Lett.* 2009 Mar;102:096803.

[89] Zheng XH, Rungger I, Zeng Z, Sanvito S. Effects induced by single and multiple dopants on the transport propertiesin zigzag-edged graphene nanoribbons. *Phys Rev B.* 2009 Dec;80:235426.

UNCORRECTED PROOFS

[90] Cruz-Silva E, Barnett ZM, Sumpter BG, Meunier V. Structural, magnetic, and transport properties of substitutionally doped graphene nanoribbons from first principles. *Physical Review B.* 2011;83:155445.
[91] Elias DC, Nair RR, Mohiuddin TMG, Morozov SV, Blake P, Halsall MP, et al. Control of graphene's properties by reversible hydrogenation: evidence for graphane. *Science.* 2009;323(5914):610–613.
[92] Soriano D, Munoz-Rojas F, Fernandez-Rossier J, Palacios JJ. Hydrogenated graphene nanoribbons for spintronics. *Physical Review B.* 2010;81(16):165409.
[93] Gunlycke D, Li J, Mintmire JW, White CT. Altering low-bias transport in zigzag-edge graphene nanostrips with edge chemistry. *Applied Physics Letters.* 2007;91(11):112108.
[94] Lopez-Bezanilla A, Triozon F, Roche S. Chemical functionalization effects on armchair graphene nanoribbon transport. *Nano Letters.* 2009;9(7):2537–2541.
[95] Cantele G, Lee YS, Ninno D, Marzari N. Spin channels in functionalized graphene nanoribbons. *Nano Letters.* 2009;9(10):3425–3429.
[96] Gorjizadeh N, Farajian AA, Esfarjani K, Kawazoe Y. Spin and band-gap engineering in doped graphene nanoribbons. *Physical Review B.* 2008;78(15):155427.
[97] Sofo JO, Chaudhari AS, Barber GD. Graphane: A two-dimensional hydrocarbon. *Phys Rev B.* 2007 Apr;75:153401.
[98] Rigo VA, Martins TB, da Silva AJR, Fazzio A, Miwa RH. Electronic, structural, and transport properties of Ni-doped graphene nanoribbons. *Physical Review B.* 2009;79(7):075435.
[99] Costa Girão E, Liang L, Cruz-Silva E, Souza Filho AG, Meunier V. Structural and electronic properties of carbon nanowiggles. *Phys Rev B*, in press. 2012;.
[100] Chen Y, Jayasekera T, Calzolari A, Kim KW, Nardelli MB. Thermoelectric properties of graphene nanoribbons, junctions and superlattices. *Journal of Physics-Condensed Matter.* 2010;22(37).
[101] Huang W, Wang JS, Liang G. Theoretical study on thermoelectric properties of kinked graphene nanoribbons. *Physical Review B.* 2011;84(4):045410.
[102] Pedersen TG, Flindt C, Pedersen J, Mortensen NA, Jauho AP, Pedersen K. Graphene antidot lattices: Designed defects and spin qubits. *Physical Review Letters.* 2008;100(13):136804.
[103] Hatanaka M. Band structures of porous graphenes. *Chemical Physics Letters.* 2010;488(4-6):187–192.
[104] Baskin A, Kral P. Electronic structures of porous nanocarbons. *Scientific Reports.* 2011;1:36.
[105] Saffarzadeh A, Farghadan R. A spin-filter device based on armchair graphene nanoribbons. *Applied Physics Letters.* 2011;98(2):023106.
[106] Wang ZF, Shi QW, Li Q, Wang X, Hou JG, Zheng H, et al. Z-shaped graphene nanoribbon quantum dot device. *Applied Physics Letters.* 2007;91(5):053109.
[107] Hancock Y, Saloriutta K, Uppstu A, Harju A, Puska MJ. Spin-dependence in asymmetric, v-shaped-notched graphene nanoribbons. *Journal of Low Temperature Physics.* 2008;153(5-6):393–398.
[108] Sevinçli H, Topsakal M, Ciraci S. Superlattice structures of graphene-based armchair nanoribbons. *Physical Review B.* 2008;78(24):245402.

UNCORRECTED PROOFS

JWST348-c14 JWST348-Jiang May 31, 2013 11:34 Printer Name: Markono Trim: 244mm × 170mm

[109] Topsakal M, Sevincli H, Ciraci S. Spin confinement in the superlattices of graphene ribbons. *Applied Physics Letters.* 2008;92(17):173118.
[110] Ma Z, Sheng W. A spin-valve device based on dumbbell-shaped graphene nanoislands. *Applied Physics Letters.* 2011;99(8):083101.
[111] Botello-Mendez AR, Cruz-Silva E, Romo-Herrera JM, Lopez-Urias F, Terrones M, Sumpter BG, et al. Quantum transport in graphene nanonetworks. *Nano Letters.* 2011;11(8):3058–3064.
[112] Girão EC, Souza Filho AG, Meunier V. Electronic transmission selectivity in multiterminal graphitic nanorings. *Applied Physics Letters.* 2011;98(11):112111.
[113] Caetano EWS, Freire VN, dos Santos SG, Albuquerque EL, Galvão DS, Sato F. Defects in graphene-based twisted nanoribbons: structural, electronic, and optical properties. *Langmuir.* 2009;25(8):4751–4759.
[114] Korte AP, van der Heijden GHM. Curvature-induced electron localization in developable Möbius-like nanostructures. *Journal of Physics: Condensed Matter.* 2009;21(49):495301.
[115] Kharche N, Zhou Y, O'Brien KP, Kar S, Nayak SK. Effect of layer stacking on the electronic structure of graphene nanoribbons. *ACS Nano.* 2011;5(8):6096–6101.
[116] Padilha JE, Lima MP, da Silva AJR, Fazzio A. Bilayer graphene dual-gate nanodevice: An *ab initio* simulation. *Physical Review B.* 2011;84:113412.
[117] Bell LE. Cooling, heating, generating power, and recovering waste heat with thermoelectric systems. *Science.* 2008;321(5895):1457–1461.
[118] Vining CB. An inconvenient truth about thermoelectrics. *Nature Materials.* 2009;8(2):83–85.
[119] Dresselhaus MS, Chen G, Tang MY, Yang R, Lee H, Wang D, et al. New directions for low-dimensional thermoelectric materials. *Advanced Materials.* 2007;19(8):1043–1053.
[120] Gunst T, Markussen T, Jauho AP, Brandbyge M. Thermoelectric properties of finite graphene antidot lattices. *Physical Review B.* 2011;84(15):155449.
[121] Saha KK, Markussen T, Thygesen KS, Nikolić BK. Multiterminal single-molecule–graphene-nanoribbon junctions with the thermoelectric figure of merit optimized via evanescent mode transport and gate voltage. *Physical Review B.* 2011;84(4):041412.
[122] Mazzamuto F, Nguyen VH, Apertet Y, Caër C, Chassat C, Saint-Martin J, et al. Enhanced thermoelectric properties in graphene nanoribbons by resonant tunneling of electrons. *Physical Review B.* 2011;83(23):235426.
[123] Dragoman D, Dragoman M. Giant thermoelectric effect in graphene. *Appl Phys Lett.* 2007;91:203116.
[124] Balandin AA, Ghosh S, Bao W, Calizo I, Teweldebrhan D, Miao F, et al. Superior thermal conductivity of single-layer graphene. *Nano Letters.* 2008;8(3):902–907.
[125] Seol JH, Jo I, Moore AL, Lindsay L, Aitken ZH, Pettes MT, et al. Two-dimensional phonon transport in supported graphene. *Science.* 2010;328(5975):213–216.
[126] Mingo N, Esfarjani K, Broido D, Stewart D. Cluster scattering effects on phonon conduction in graphene. *Physical Review B.* 2010;81(4):045408.
[127] Wei N, Xu L, Wang HQ, Zheng JC. Strain engineering of thermal conductivity in graphene sheets and nanoribbons: a demonstration of magic flexibility. *Nanotechnology.* 2011;22:105705.

UNCORRECTED PROOFS

[128] Hu J, Schiffli S, Vallabhaneni A, Ruan X, Chen YP. Tuning the thermal conductivity of graphene nanoribbons by edge passivation and isotope engineering: A molecular dynamics study. *Applied Physics Letters.* 2010;97:133107.
[129] Tan ZW, Wang JS, Gan CK. first-principles study of heat transport properties of graphene nanoribbons. *Nano Letters.* 2011;11(1):214–219.
[130] Ni X, Liang G, Wang JS, Li B. Disorder enhances thermoelectric figure of merit in armchair graphane nanoribbons. *Applied Physics Letters.* 2009;95:192114.
[131] Haskins JB, Kinaci A, Sevik C, Sevincli H, Cuniberti G, Cagin T. Control of thermal and electronic transport in defect-engineered graphene nanoribbons. *ACS Nano.* 2011;5:3779–3787.
[132] Mazzamuto F, Saint-Martin J, Nguyen V, Chassat C, Dollfus P. Thermoelectric performance of disordered and nanostructured graphene ribbons using Green's function method. *Journal of Computational Electronics.* 2012;11:67–77. 10.1007/s10825-012-0392-0.
[133] Nikolic BK, Saha KK, Markussen T, Thygesen KS. First-principles quantum transport modeling of thermoelectricity in single-molecule nanojunctions with graphene nanoribbon electrodes. *Journal of Computational Electronics.* 2012 Mar;11(1):78–92.
[134] Sevinçli H, Cuniberti G. Enhanced thermoelectric figure of merit in edge-disordered zigzag graphene nanoribbons. *Phys Rev B.* 2010 Mar;81:113401.
[135] Chang PH, Nikolic BK. Edge currents and nanopore arrays in zigzag and chiral graphene nanoribbons as a route toward high-ZT thermoelectrics. *Phys Rev B.* 2012 Jul(4); 16;86.

UNCORRECTED PROOFS